J Appl Electrochem (2008) 38:907–913
DOI 10.1007/s10800-008-9494-6

ORIGINAL PAPER

Electrochemical performance of mechanically treated SnO_2 powders for OER in acid solution

S. Palmas · A. M. Polcaro · F. Ferrara · J. Rodriguez Ruiz · F. Delogu · C. Bonatto-Minella · G. Mulas

Received: 14 September 2007 / Revised: 17 January 2008 / Accepted: 21 January 2008 / Published online: 5 February 2008

Abstract Commercial tin dioxide powders have been subjected to mechanical treatment in order to modify their microstructure. Processed powders were then used to assembly thin film electrodes which worked as anodes in a three electrode cell to drive the oxygen evolution reaction from acid solution. Cyclic voltammetry and polarization experiments were carried out together with electrochemical impedance spectroscopy to highlight the effects of milling on the catalytic performance. The findings suggest that the mechanical processing is capable of generating a considerable amount of lattice defects. The grain boundary extension as well as the content of structural disorder increase with the processing time. The increase in both the reactive site density and extent of structural disorder results in an enhanced chemical reactivity of the assembled electrodes.

Keywords Ball milling · BDD/SnO_2 electrodes · Electrochemical impedance spectroscopy · Nanoparticles · Oxygen evolution reaction

1 Introduction

The mechanical processing of powders in ball mills is a simple technique to carry out thermodynamically unfavoured reactions and destabilize equilibrium compounds [1, 2]. Metastable phases such as amorphous alloys and nanostructured systems can be easily produced as a consequence of the far-from-equilibrium processing conditions [2]. These determine the excitation of unusual states of reactivity via the application of mechanical forces and the consequent transfer of mechanical energy [2–5].

The transfer of energy to powders takes place at impact events in which a relatively small fraction of the total powder charge is trapped between colliding surfaces [6]. Repeatedly involved in collisions, powder particles undergo cold-welding, fracturing and plastic deformation processes [6, 7]. Whereas the former induce a variation of number and morphology of powder particles [7], local deformation processes result in a decrease in the average crystallite size and accumulation of lattice disorder [6]. The gradual modification of microstructure, with formation of grain boundaries and successive refinement of coherent crystalline domains down to the nanometer range can, in turn, promote phase transitions and chemical transformations as well as significant changes of physical properties [2–7].

At microscopic level, the apparent simplicity of mechanical treatment is replaced by a remarkable complexity originating from intertwined atomistic processes still awaiting a satisfactory description and rationalization [8–15]. For example, the intimate nature of the local excited states appearing in solid phases as a result of applied mechanical forces is still debated [8–15]. A comprehensive conceptual approach to transformation kinetics is still lacking even though any progress in such a direction could open the door, not only to a deeper understanding of atomistic processes but also to practical applications [2–7].

The present work focuses on the electrochemical performance of electrodes obtained by assembling SnO_2

S. Palmas (✉) · A. M. Polcaro · F. Ferrara · J. Rodriguez Ruiz · F. Delogu
Dipartimento di Ingegneria Chimica e Materiali, Università degli Studi di Cagliari, Piazza d'Armi, 09123 Cagliari, Italy
e-mail: sipalmas@dicm.unica.it

C. Bonatto-Minella · G. Mulas
Dipartimento di Chimica, Università degli Studi di Sassari, Via Vienna 2, 07100 Sassari, Italy

powders, mechanically processed for different times, on boron doped diamond (BDD) supports. BDD has been chosen in the light of its chemical inertness, very low background current and large potential difference between hydrogen and oxygen evolution and an extreme resistance to chemical and electrochemical attack [16]. Its outstanding properties also make it an attractive substrate for electrochemical characterisation of supported electrocatalytic particles, avoiding the problems encountered with other common substrates. The choice of SnO_2 is motivated by its wide use in both fundamental and applicative studies [17]. For example, RuO_2–SnO_2, IrO_2–SnO_2, RuO_2–TiO_2–SnO_2, IrO_2–TiO_2–SnO_2 and RuO_2–Sb_2O_5–SnO_2 systems are often adopted to improve the electrode performance for O_2 evolution in acid media. In these cases the use of SnO_2 represents the search for a compromise between electrocatalytic activity, long-term electrode stability and cost. It is a relatively cheap oxide capable of stabilizing the electrode and partly producing catalytic effects.

The SnO_2-based electrodes prepared in the present work have been used to obtain information on the electrochemical properties of mechanically-processed powders and, in turn, on the modification of their chemical reactivity as a consequence of the accumulation of lattice defects.

2 Experimental section

2.1 Preparation of powders

High purity SnO_2 commercial powders (Aldrich, 99.99%, 325 mesh) were used. The mechanical treatment was carried out with a commercial Spex/Mixer Mill mod. 8000. Powder amounts of 8 g were introduced into a stainless steel vial with two stainless steel balls. The vial was then fixed on the mechanical arm and the mill operated at about 14.6 Hz. The treatment was interrupted after selected time intervals to empty the vial and refill it with a further 8 g of untreated powder. The powders extracted from the vials were then compacted to prepare disk-shaped samples for X-ray diffraction (XRD).

2.2 Powder characterization

XRD analyses were performed on a Rigaku D/Max diffractometer equipped with a Cu radiation tube and a graphite monochromator in the diffracted beam. The XRD patterns of the SnO_2 powders were accurately analyzed by applying the well known Rietveld method [18]. This allowed a numerical reconstruction of the observed experimental XRD patterns via a best-fitting procedure involving the parameters characteristic of the set of mathematical functions employed to reproduce the peak profiles [18]. It was thus possible to estimate the average size L of coherent diffraction domains and the concentration of structural defects, quantified by the so-called microstrain content ε [18, 19].

The experimental XRD pattern of powders milled for 3 h is shown in Fig. 1, together with numerically refined peak profiles.

The structural evolution of SnO_2 powders is illustrated from the average crystallite size L and microstrain ε values reported in Fig. 2 as a function of the milling time, t. It can be seen that, as expected, the gradual L decrease is paralleled by a progressive increase of ε.

The decrease in the average size of single crystallites is therefore accompanied by the accumulation of structural disorder due to the generation of a far-from-equilibrium population of lattice defects such as vacancies, interstitials, dislocations and grain boundaries.

2.3 Electrode assembly

The electrochemical response of powder samples processed for 3, 16 and 24 h, hereafter referred to as S3, S16 and S24 respectively, has been compared with that of untreated powders, hereafter referred to as NM. Powders were assembled onto the surface of BDD supports to obtain thin film electrodes. More specifically, 14 mg of powders were added to 1 cm^3 of distilled water and the system was subjected to ultrasonic treatment for 30 min to suitably disaggregate powder particles and disperse them in the liquid. About 0.2 cm^3 of the suspension were then used to cover a BDD electrode surface with geometric area of

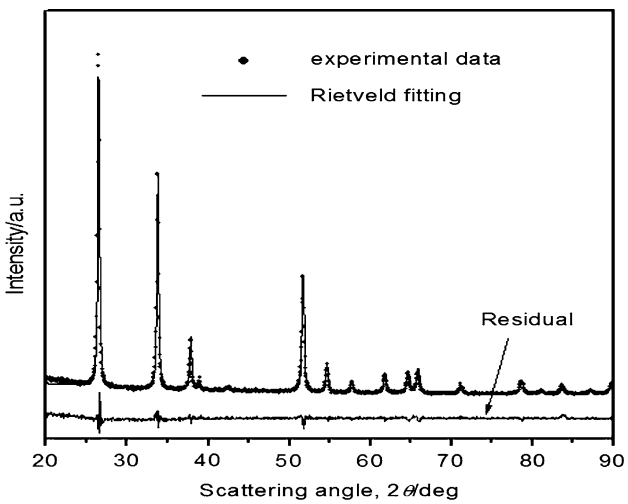

Fig. 1 The experimental XRD pattern of SnO_2 powders milled 3 h as a function of the scattering angle 2θ. The best-fitted numerically reconstructed Rietveld pattern and the residual trace are also shown

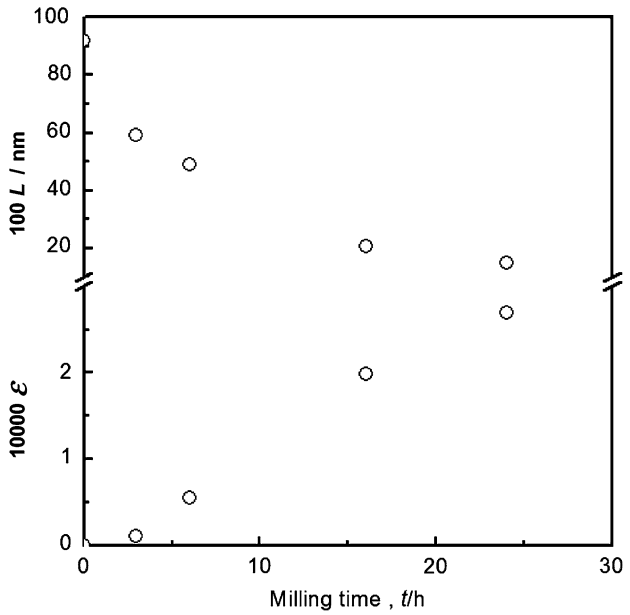

Fig. 2 The average crystallite size L and microstrain ε as a function of the milling time t

1 cm^2. Finally, the suspension was dried for 30 min at 80 °C in an oven. Approximately 2 mg of SnO_2 were thus deposited per square centimetre. The obtained oxide films were stable up to potentials of the order of 2.3–2.5 V, above which O_2 bubbling resulted in film rupture and detachment.

2.4 Electrochemical cell

Experimental runs were performed in a conventional three-electrode cell in which the BDD/SnO_2 electrode worked as anode and a large platinum sheet as counter electrode. The reference was a saturated calomel electrode (SCE) connected to the cell by a Luggin capillary to minimize uncompensated ohmic drops. All the potential values hereafter quoted are referred to SCE.

2.5 Electrochemical measurements

A potentiostat (Model 7050 AMEL) and a frequency response analyser (FRA, Model 7200 AMEL) were used to perform voltammetric, polarization and spectroscopic analyses. Runs were carried out in aqueous solutions of H_2SO_4 at a concentration of 0.5 M. The potential interval explored during the course of voltammetric measurements ranged between the open circuit voltage (OCV), typically between 0.1 and 0.2 V, and 2.5 V. Negative potential values have been also occasionally imposed to investigate the possible occurrence of SnO_2 phase transformations.

Quasi steady-state polarisation runs were also carried out in the same potential range, the potential scan rate being 1 mV s^{-1}.

Electrochemical impedance spectroscopy measurements were performed by superimposing a sinusoidal signal with excitation amplitude of 10 mV at different bias potentials in the range from 0 to 2 V. Impedance spectra were recorded in the frequency range 0.1 to 1×10^5 Hz by collecting 16 points per decade. Zassist and ZsimpWin softwares were used, respectively, to drive the experiments and fit the resulting curves to suitable equivalent circuits.

3 Results and discussion

3.1 Electrochemical characterization of the samples

A typical example of the curves obtained from cyclic voltammetry on NM powders in aqueous solution 0.5 M H_2SO_4 is reported in Fig. 3. Aimed at pointing out the phase transitions possibly undergone by SnO_2 powders, a voltammetric cycle was performed with $E_0 = \text{OCV}$, $E_1 = -1$ V and $E_2 = 2.5$ V.

In accordance with literature [20], at a potential value of about −0.6 V the reduction of Sn (IV) to Sn (0) is observed. Oxidation to Sn (II) and Sn (IV) is then observed at about −0.4 V and 1.1 V, respectively. The O_2 evolution process is finally detected at higher anodic potentials.

As often pointed out [21–23], the mechanism of O_2 evolution at oxide electrodes is complicated and its full characterization and rationalization still challenge electrochemists. The reaction is typically a multi-stage one, the rate determining step depending on the strength of the intermediate product adsorption. In turn, this is governed

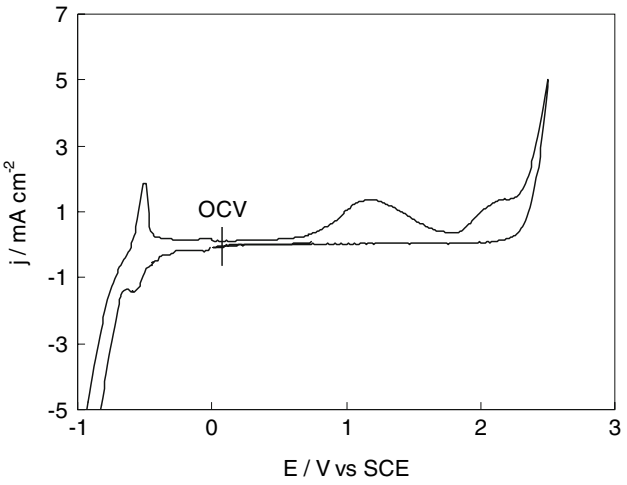

Fig. 3 Typical curves for cyclic voltammetry at NM powder electrodes performed with $E_0 = \text{OCV}$, $E_1 = -1$ V and $E_2 = 2.5$ V. Scan rate 100 mV s^{-1}

by the oxide layer composition [21]. A detailed study has been carried out on PbO_2 [22] which is referred as an "non-active" oxide, as is the case of SnO_2. The reactivity of these species is mainly ascribed to the formation of a hydrated oxide layer containing sites able to bind hydroxide radicals $HO^{\bullet}$ during the course of O_2 evolution. Despite the process being a remarkably complex one, the following simplified mechanism has been proposed for the reaction taking place in acid medium [22, 23]:

$$SnO_2 + H_2O \rightarrow SnO_2(HO^{\bullet}) + H^+ + e^- \quad (1)$$

$$SnO_2(HO^{\bullet}) \rightarrow SnO_2 + H^+ + O + e^- \quad (2)$$

$$2O \rightarrow O_2 \quad (3)$$

$SnO_2(HO^{\bullet})$ stands for the active site binding the $HO^{\bullet}$ species. According to such a mechanism, the peak detected in the voltammetric curve (Fig. 3) before the current rise related to O_2 evolution can be ascribed to the intermediate stages of this latter process. The current density j measured at the potential E of 2 V for the different powder samples as a function of the milling time t is given in Fig. 4. The average specific surface area of crystallites S_p has also been reported for sake of comparison. S_p was evaluated according to the general expression:

$$S_p = \frac{f}{\rho L} \quad (4)$$

where ρ is the SnO_2 density and f a shape factor. Under the simplifying assumption that powder particles have spherical shape, f was set equal to 6.

It can be seen that both quantities change linearly with t, thus suggesting a possible direct correlation. Although the direct correlation between the total surface area of crystallites S_p and the current density j only suggests an increase in the total number of active surface sites, with no evidence of significantly different reactivity, this latter possibility cannot be excluded a priori. Actually, it is expected that the chemical reactivity of surface sites pertaining to powders subjected to mechanical treatment is higher than that of surface sites in untreated powders. Further investigations were then carried out to specifically address this point.

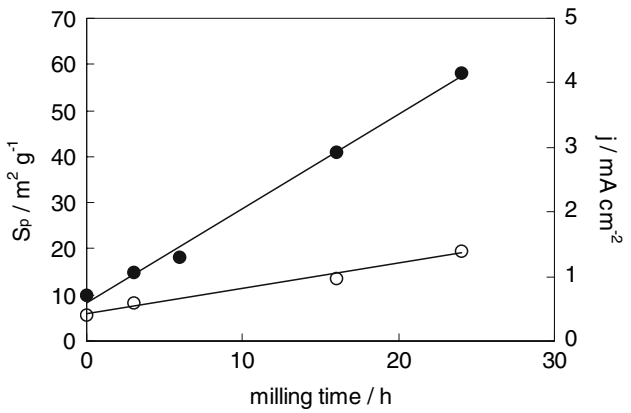

Fig. 4 Specific surface area of crystallites S_p (●) and electric current density j (◯) measured at $E = 2$ V as a function of the milling time t

Polarization experiments were performed in the potential range between 1.5 and 2.5 V, the quasi steady-state current-potential data being recorded at a rate of 1 mV s^{-1}. As widely discussed [24], the Tafel plot provides only limited information on the reaction mechanism when electrode reactions take place at very high potential as in the case of O_2 and O_3 evolution, so that b values very different from the theoretical ones have often been obtained [25]. Nevertheless, in the present case a comparison between the behaviour of the different powder samples can still give useful information on their electrochemical catalytic activity. The Tafel parameters, a and b, together with the exchange current density j_0 are quoted in Table 1.

The j_0 value increases with milling time t, thus indicating a larger electrochemical catalytic activity for powders treated for longer times. It is, however, worth noting that j_0 is measured relative to the electrode geometrical surface area, which is only an apparent surface area. The differences in a values for powder samples processed for different milling times could be then due to the comminution process accompanying the mechanical treatment. In order to obtain a more representative quantity, data have been therefore normalised to the specific surface area of crystallites S_p obtained from XRD measurements. The resulting a^* and j_0^* values for the different samples, also reported in Table 1, are still characterized by significant differences, particularly between the S24 sample and the remaining ones. This suggests that the mechanical processing not only determines an increase in the total surface area, and then of the number of active sites, but also modifies their nature.

3.2 Electrochemical impedance spectroscopy

The results obtained from electrochemical impedance spectroscopy on the NM samples at different potentials are shown in Fig. 5 as a Nyquist plot.

Table 1 Values of Tafel parameters obtained at different samples

	b (mV dec^{-1})	a (V)	a^* (V)	j_o (mA cm^{-2})	j_0^* (mA cm^{-2})
NM	196	1.423	1.089	5.61×10^{-8}	2.80×10^{-10}
S3	212	1.35	1.070	4.29×10^{-7}	8.97×10^{-10}
S16	228	1.314	1.064	1.76×10^{-6}	2.20×10^{-9}
S24	251	0.831	0.602	4.83×10^{-4}	3.97×10^{-7}

The asterisked values are derived from current density values normalised with respect to S_p

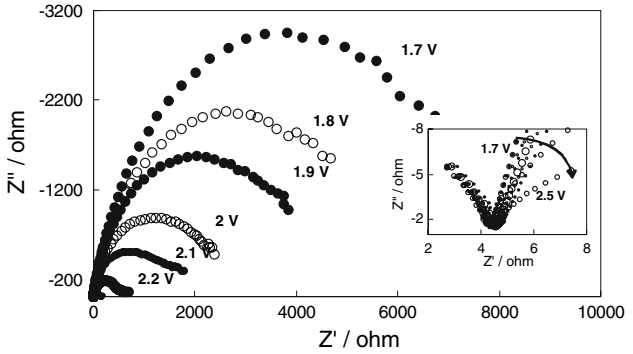

Fig. 5 Electrochemical impedance spectroscopy curves obtained at NM samples at the different potential values. The inset reports a close-up view of the high frequency region

As shown in the inset, a capacitive loop independent of potential is always observed in the high frequency region. Two other loops are detected in the lower frequency region, the resolution of which depends on the potential applied. Highest impedance values are observed at less positive potential and their values decrease progressively as the potential increases. Correspondingly, the capacitive loops become better defined and the polarization resistances R_p for the OER, calculated by the low-frequency cut off of the curves on the real axis, decrease exponentially with applied potential according to a Buttler Volmer trend [26].

The polarization resistance R_p values can be adopted to support the experimental findings relative to the polarization curves. The polarization resistance can be expressed as:

$$R_p = \frac{\partial \eta}{\partial j} = \frac{b}{j_0} \exp\left(\frac{-2.3}{b}\eta\right) \tag{5}$$

It follows that:

$$\eta = b \log\left(\frac{1}{R_p}\right) - b \log\left(\frac{j_0}{b}\right) \tag{6}$$

Accordingly, a plot of η vs. $\log\left(R_p^{-1}\right)$ gives the Tafel slope. The trend of η vs. $\log\left(R_p^{-1}\right)$ (curve a) obtained for NM sample is given in Fig. 6 together with the Tafel plot (curve b).

A b value of 195 mV dec^{-1} was calculated by fitting experimental data from impedance spectroscopy with Eq. 6, which well agrees with the corresponding value obtained from the polarization curve (Table 1).

An example of the Nyquist diagrams obtained for the different electrodes at a potential of 2 V is shown in Fig. 7.

With the aim of carrying out a quantitative analysis of the experimental results obtained, the electrochemical response of the electrodes has been modelled according to the equivalent electrical circuit approach. To this end, in accordance with the aforementioned mechanism for O_2 evolution illustrated by Eqs. 1–3, the faradaic current i_F has been considered dependent on both the applied potential and an additional variable, θ, representing a measure of the

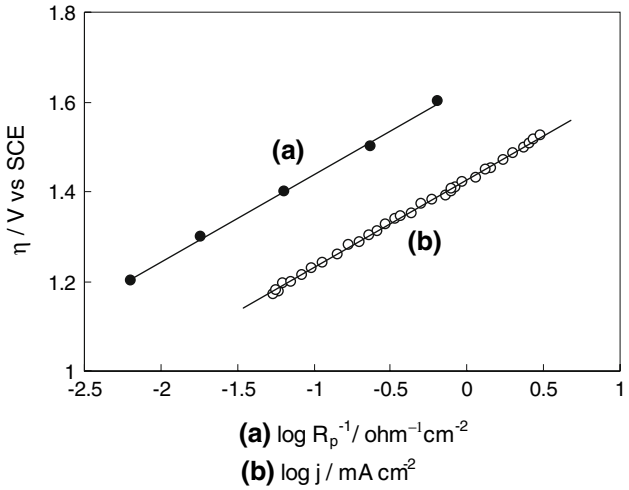

Fig. 6 Tafel plots for NM sample: (a) η vs. $\log\left(R_p^{-1}\right)$ from impedance data, (b) η vs. $\log j$ from quasi steady-state data

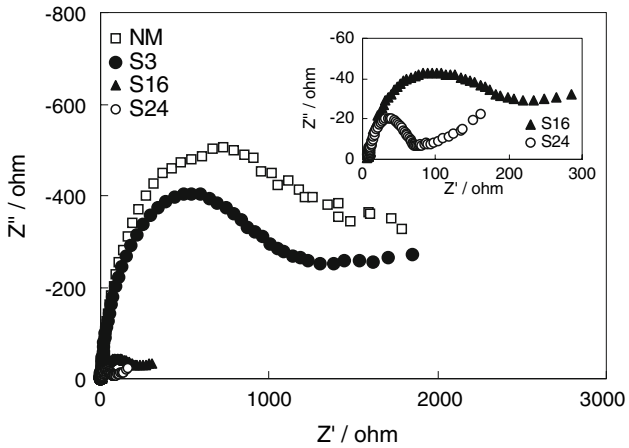

Fig. 7 Nyquist plots obtained at a potential of 2 V for the different samples. The inset shows a close-up view of the low impedance region

reaction intermediate $SnO_2(HO^{\bullet})$ surface coverage. Following previous work [27], the faradaic admittance, Y_F, of an electrode reaction with one state variable besides electrode potential can be written as:

$$Y_F = \frac{1}{R_{ct}} + \frac{B}{A + j\varpi} \tag{7}$$

where

$$\frac{1}{R_{ct}} = \left(\frac{\partial i_F}{\partial E}\right)_{ss} \tag{8}$$

$$B = \left(\frac{\partial i_F}{\partial \theta}\right)_{ss} \left(\frac{\partial \dot{\theta}}{\partial E}\right)_{ss} \tag{9}$$

$$A = -\left(\frac{\partial \dot{\theta}}{\partial \theta}\right)_{ss} \tag{10}$$

Here R_{ct} is the transfer resistance of the electrode reaction and the subscript ss stands for steady state. As mentioned above, θ is the reaction intermediate $SnO_2(HO^{\bullet})$ surface coverage, whereas $\dot{\theta}$ is its change rate $d\theta/dt$.

On the other hand, it is well established that a general equivalent circuit for the faradaic electrode process involving one state variable can be represented by the schematic quoted in Fig. 8.

The total impedance Z of the electrode process can be expressed by

$$Z = R_s + \frac{1}{Y_F + j\varpi C_{dl}} \tag{11}$$

where C_{dl} is the double-layer capacitance, R_s the uncompensated solution resistance and Y_F the faradaic admittance. The faradaic impedance Z_F can be written as:

$$Z_F = \frac{1}{Y_F} = R_{ct} + \frac{R_a}{1 + j\varpi R_a C_a} \tag{12}$$

R_a and C_a represent, respectively, the equivalent resistance and capacitance associated with the intermediate adsorption.

The relationship between the electrical elements in the equivalent circuit and the electrochemical parameters in the faradaic admittance can be pointed out by comparing Eqs. 7 and 12. Accordingly:

$$B = \frac{-1}{R_{ct}^2 C_a} \tag{13}$$

$$A = \frac{1}{C_a}\left(\frac{1}{R_a} + \frac{1}{R_{ct}}\right) \tag{14}$$

It follows that two capacitive loops must be expected in impedance diagrams connected with the faradaic process. An additional element was added to the equivalent electrical circuit to take into account the capacitive response of the oxide film. This modifies the equivalent circuit shown in Fig. 8 into that schematically depicted in Fig. 9.

Constant phase elements (CPEs) were used instead of capacitors (C) to fit experimental data. According to literature [28–30], using CPEs is a good approach for studying solid electrodes with different degrees of surface roughness and non-uniform structure or distribution of reactive surface sites. The CPE impedance can be expressed as

$$Z_{CPE} = \frac{1}{Q(j\varpi)^n} \tag{15}$$

Q representing the capacity parameter expressed in S cm^{-2} s^n and n accounting for the deviation from the ideal behaviour, n being 1 for a perfect capacitor.

Figure 10 depicts an example of the fit between experimental data and fitting curves based on the complex nonlinear least squares (CNLS) method for the sample NM.

The equivalent circuit parameter values obtained for the different samples at a potential E value of 2 V are quoted in Table 2.

It can be seen that the film resistance increases with the milling time t: the mechanical treatment leads to a comminution of powder particles, with a corresponding increase of the specific free surface, and an increase in their lattice defect content. The decrease in average crystallite size corresponds to an increase in grain boundary extension area. As a consequence, the intensity of scattering events involving charge carriers at grain boundaries also increases. A decrease of the overall charge carrier mobility is therefore observed and, in turn, an electrical resistivity increase [31]. The formation of highly defective grain boundaries is further highlighted [28–30] by the decreasing CPE exponent of the electrical element connected with the reaction intermediate $SnO_2(HO^{\bullet})$ absorption: high values of n are measured for samples milled up to 3 h which becomes 0.46 for sample S24.

Additional evidence of the capability of mechanical processing of enhancing the chemical reactivity of powders

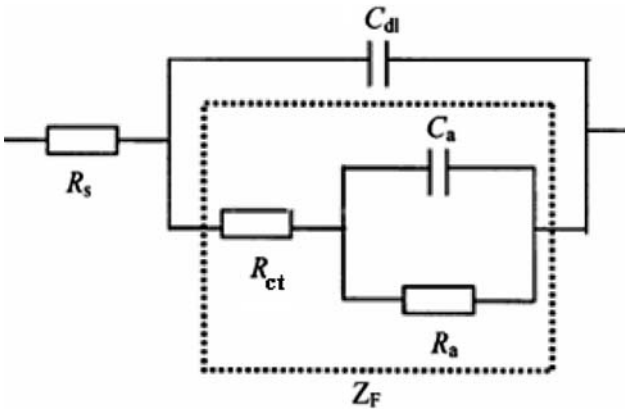

Fig. 8 Equivalent electric circuit for oxide electrodes during O_2 evolution reaction

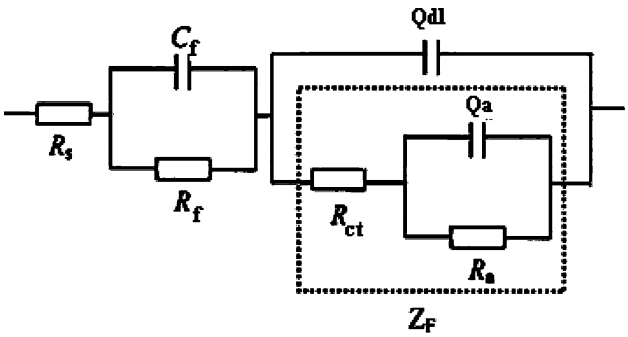

Fig. 9 Modified equivalent electric circuit for oxide electrodes during O_2 evolution reaction

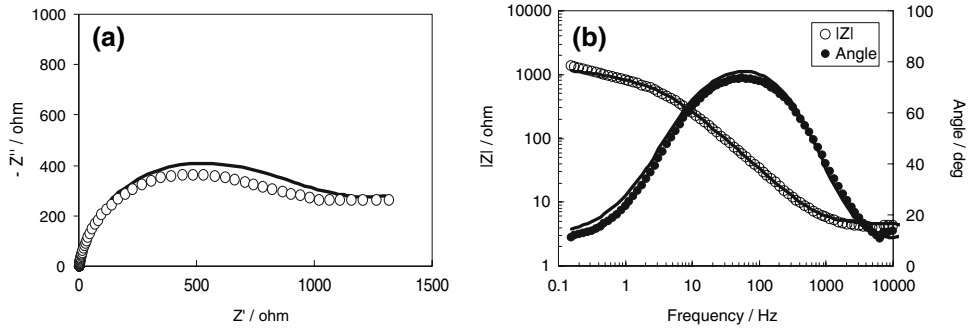

Fig. 10 Example of the fit between calculated and experimental Nyquist (**a**) and Bode (**b**) modulus and phase angle plots at $E = 2$ V

Table 2 Values of the parameters of the equivalent electrical circuit reported in Fig. 9, derived for the different samples from runs performed at $E = 2$ V vs. SCE

	NM	S3	S16	S24
R_s (ohm)	0.2	0.03	0.01	0.01
C_f (μF)	0.4	0.7	0.2	0.1
R_f (ohm)	4.0	4.4	8.3	9.7
Q_{dl} (μS s^n)	60	54	27	34
n	0.96	0.94	0.97	1
R_{ct} (ohm)	800.5	782.2	45.7	26.3
Q_a (mS s^n)	0.3	0.5	0.4	2.1
n	0.90	0.96	0.64	0.46
R_a (ohm)	1002.1	725.4	164.1	50.9

via the disordering of crystalline lattice is provided by the progressively decreasing R_{ct} and R_a values.

4 Conclusions

The present work represents a preliminary investigation of the electrochemical properties of tin dioxide powders subjected to mechanical processing, used as electrodes for oxygen evolution reaction in acid medium. Cyclic voltammetry, electrical polarization and electrochemical impedance spectroscopy experiments have been carried out to gain information on the mechanistic scenario underlying the chemical reaction and, indirectly, on the modifications connected with powder particle deformation. This latter determined a significant decrease in the average crystallite size and the accumulation of structural disorder. According to the equivalent circuit approach, such processes result in an increase in the thin film resistance. The larger grain boundary extension related to the crystallite size decrease determined a corresponding decrease in the charge carrier mobility. At the same time, evidence has been collected suggesting that the enhanced catalytic activity of processed powders can be related, not only to the grain boundary extension increase, but also to the generation of surface active sites with different reactivity. Further work is needed to support the aforementioned preliminary conclusions.

Acknowledgements Prof. G. Cocco, Department of Chemistry, University of Sassari, Italy, is gratefully acknowledged for useful suggestions. Financial support was given by the Universities of Cagliari and Sassari.

References

1. Siegel RW, Hu E, Roco MC (eds) (1999) Nanostructure science and technology. WTEC, Loyola College, Maryland
2. Suryanarayana C (2001) Prog Mater Sci 46:1
3. Butyagin PYu (1989) Sov Sci Rev B Chem 14:1
4. Gutman EM (1998) Mechanochemistry of materials. Cambridge International Science Publishing, Cambridge
5. Urakaev FKh, Boldyrev VV (2000) Powder Technol 107:93
6. Delogu F, Deidda C, Mulas G, Schiffini L, Cocco G (2004) J Mater Sci 39:1
7. Courtney TH (1995) Mater Trans JIM 36:110
8. Bellon P, Averback RS (1995) Phys Rev Lett 74:1819
9. Hoagland RG, Baskes MI (1998) Scr Mater 39:417
10. Fu XY, Falk ML, Rigney DA (2001) Wear 250:420
11. Lund AC, Schuh CA (2003) Appl Phys Lett 82:2017
12. Butyagin PYu, Streletskii AN (2005) Phys Solid State 47:856
13. Levitas VI (2004) Phys Rev B 70:184118
14. Odunuga S, Li Y, Krasnochtchekov P, Bellon P, Averback RS (2005) Phys Rev Lett 95:045901
15. Delogu F, Mulas G, Enzo S, Schiffini L, Cocco G (2007) Chem Sust Develop 15:157
16. Pleskov YV (1999) Russ Chem Rev 68:381
17. Batzill M, Diebold U (2005) Prog Surf Sci 79:47
18. Lutterotti L, Ceccato R, Dal Maschio R, Pagani E (1998) Mater Sci Forum 278:87
19. Klug HP, Alexander LE (1974) X-Ray diffraction procedures. Wiley-Interscience, New York
20. Patil PS, Chigare PS, Sadale SB, Mujawar SH, Shinde PS (2007) Sol Energy Mater Sol Cells 91:859
21. Martelli GN, Ornelas R, Faita G (1994) Electrochim Acta 39:1551
22. Amadelli R, Maldotti A, Molinari A, Danilov FI, Velichenko AB (2002) J Electroanal Chem 534:1
23. Al faro MAQ, Ferro S, Martinez-Huitle CA, Vong YM (2006) J Braz Chem Soc 17:227
24. Li FB, Hillman R, Lubetkin SD (1992) Electrochim Acta 37:2723
25. Fernandes KC, Da Silva LM, Boodts JFC, De Faria LA (2006) Electrochim Acta 51:2809
26. Meilin L, Zhonglin W (1998) Solid State Ionics 107:105
27. Cao CN (1990) Electrochim Acta 35:831
28. Rammelt U, Reinhard G (1990) Electrochim Acta 35:1045
29. Gudic S, Radosevic J, Kliskic M (1996) J Appl Electrochem 26:1027
30. Spataru N, Lehelloco JG, Durand R (1996) J Appl Electrochem 26:397
31. Bilgin V, Kose S, Atay F, Akyuz I (2004) Mater Lett 58:3686